Paper:

Tsunami Waveform Inversion of the 2007 Peru (M_w8.1) Earthquake

César Jiménez[*1,*2], Nabilt Moggiano[*2], Erick Mas[*3], Bruno Adriano[*3], Yushiro Fujii[*4], and Shunichi Koshimura[*3]

[*1]Universidad Nacional Mayor de San Marcos
FENLAB Av Venezuela s/n, Lima, Perú
E-mail: cjimenezt@unmsm.edu.pe
[*2]Direccion de Hidrografia y Navegacion, DHN, Chucuito-Callao, Peru
[*3]International Research Institute of Disaster Science, Tohoku University, Sendai, Japan
[*4]International Institute of Seismology and Earthquake Engineering,
Building Research Institute, Ibaraki, Japan
[Received July 1, 2014; accepted September 29, 2014]

An earthquake shook the central-southern coast of Peru on August 15, 2007, as a coseismic effect a tsunami was generated, which flooded some villages and beach resorts and killed 3 people. From the analysis and signal processing of 10 tidal records, we obtained the parameters of the seismic source and the initial coseismic deformation through an inversion modeling, in which the synthetic signals are compared with the observed signals by a non-negative least square method. The maximum slip located on the southern part of the rupture geometry is 7.0 m. The calculated scalar seismic moment is $M_0 = 1.99 \times 10^{21}$ Nm, equivalent to a magnitude of M_w8.1. We used these parameters to obtain a heterogeneous seismic source model, which was used as initial condition to simulate the tsunami propagation and inundation. We used the field survey observations to validate our source model.

Keywords: seismic source, inversion, numerical simulation

1. Introduction

The objective of the research is to obtain the slip distribution (or seismic source distribution) and deformation field of the Pisco (Peru) 2007 earthquake from tsunami waveform inversion [1] and the validation of this model from the field survey observations [2].

One way to verify a seismic source model or initial coseismic deformation model is by simulating the corresponding tsunami. The parameters such as arrival time, amplitude and polarity of the first wave and in general the tsunami waveform simulated should have a good correlation with the corresponding values digitally processed of tidal gauge records for the available stations.

From a physical point of view, the tsunami waveform inversion provides better results to obtain the initial deformation field, because the velocity of tsunami waves is relatively well known in this method (the velocity of the tsunami waves depends only on the bathymetry), unlike in teleseismic waveform inversion the velocity of the seismic waves is not very well known, it is assumed a velocity model that provides the best correlation between the observed signals and the simulated signals in the inversion process. The goodness of the results obtained depends on the quality of the tidal gauge recordings and quality of bathymetry around the tidal stations.

The Pisco earthquake of 2007 (M_w8.1) was generated at the boundary between the Nazca and South America tectonic plates. These two plates converge at a rate of 7-8 cm per year [3]. The quake is the type of thrust fault at the interface between the two plates, the Nazca plate moving beneath the South American plate, a process known as subduction. The dominant seismic activity along the coast of Peru is a direct consequence of subduction of the Nazca plate beneath the South American plate, so that the coast of Peru has a history of great earthquakes. Over the past five centuries have been many destructive earthquakes of magnitude greater than M_w8.0 in some place of Peru [4].

As coseismic effect of the earthquake, a tsunami was generated, which originated the greatest run-up south of the Paracas Peninsula, this corresponds to the greater asperity. The focal mechanism for these earthquakes generally corresponds to a thrust fault with the nodal plane oriented in the NNW-SSE and dipping nearly horizontal plane [5].

2. Data

2.1. Tidal Waves Recording

We used 12 digital tidal stations as shown in **Fig. 1** with red triangles. Eleven belonging to Sea Level Station Monitoring Facility [6], usually located in a port or coastal inlet, and one buoy DART (Deep-ocean Assessment and Reporting of Tsunamis) of the National Data Buoy Center [7] located at deep sea. All these stations are

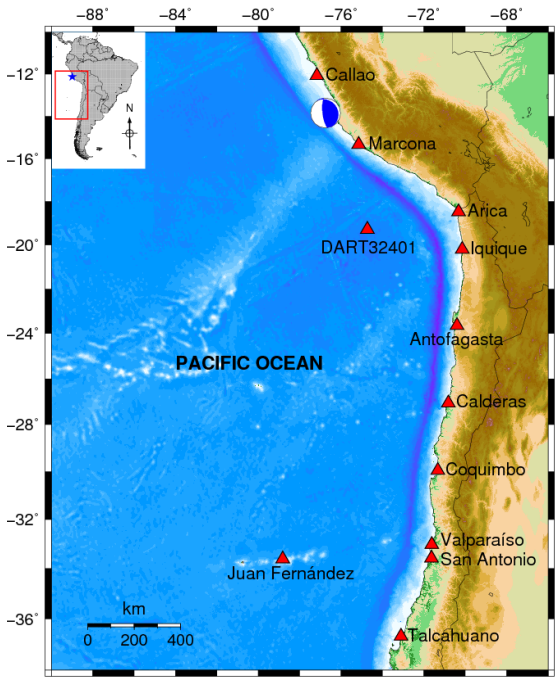

Fig. 1. Bathymetry and distribution of tidal wave stations.

located along the coast of Chile and Peru, except DART buoy (**Fig. 1**). A good azimuthal geometric distribution of stations with respect to the epicenter is obtained with additional stations to the north; however, it is not the case for this event because the missing of tidal recordings of good quality, free of noise from stations located in the near and regional field to avoid dispersion effects.

2.2. Digital Tidal Wave Processing

Each tidal gauge signals are composed of a wide range of frequencies with 3 main components: oceanic tides (of astronomical origin), waves or surge (of atmospheric origin) and tsunami (of tectonic origin, mainly). To analyze the tidal gauge records of tsunami we applied the same algorithms of digital signal processing as in Jiménez (2007) [8]. Here a brief description of the method: first the data is interpolated (in time domain) for a sampling rate of 1 minute (using the cubic interpolation method), this in order to homogenize the data, since each station can have a different sampling rate (1 min, 2 min or 5 min). Then, the mean value of the signal is removed. A high-pass Butterworth filter ($f_c = 6.94 \times 10^{-5}$ Hz) and a low-pass filter ($f_c = 0.0083$ Hz) is applied to remove components of long period (tides) and of short period (surges). Finally, the time is referenced with respect to origin time of the earthquake [9]. However, for computational purposes of the inversion process, all records (observed and calculated or Green functions) are synchronized so that the arrival time of the first wave corresponds around 20th minute, i.e., close to the lower arrival time corresponding to Marcona station (**Table 1**).

The arrival time for Marcona station is less than the arrival time of Callao station, this is due to the bathymetry and directivity of the propagation of tsunami waves. Except Marcona station, all arrival times have some proportionality to the epicentral distance of each station.

Table 1. The tidal stations are in order from north to south. The arrival time (TA) is referenced with the origin time of the earthquake.

N	Station	Lat°	Lon°	TA (min)
1	Callao	-12.071	-77.174	55
2	Marcona	-15.343	-75.157	21
3	Arica	-18.476	-70.323	80
4	DART32401	-19.287	-74.731	51
5	Iquique	-20.205	-70.148	82
6	Antofagasta	-23.653	-70.404	110
7	Caldera	-27.065	-70.825	133
8	Coquimbo	-29.950	-71.335	164
9	Valparaiso	-33.027	-71.626	187
10	San Antonio	-33.580	-71.630	197
11	Juan Fernandez	-33.620	-78.830	181
12	Talcahuano	-36.695	-73.106	254

2.3. Bathymetry

Because the speed and directivity of tsunami waves depend on the marine topography (or bathymetry), is essential to have a good model of bathymetry to calculate the inversion. The global bathymetry model is taken from GEBCO 30 [10], which has a grid resolution of 30 arc sec or ∼927 m (**Fig. 1**). For Callao station, we used a finer bathymetry (3 arc sec or 92 m), corresponding to marine soundings. However, for other stations we used a coarse bathymetry.

2.4. Rupture Geometry from Aftershocks

Hypocentral parameters taken from the National Earthquake Information Center [11] are given in **Table 2**. NEIC has recorded a total of 167 events of magnitude greater than M_w4.0, since the occurrence of main earthquake (Aug. 15, 2007) until a month later (Sep. 15, 2007). The strongest aftershock occurred on August 18, 2007 and had a magnitude of M_w6.0.

These aftershocks are distributed mainly between the trench and the coast line, and to a lesser extent on the continent, along the geometry of rupture from Cañete (13°S) to Paracas Peninsula (15°S) covering a surface with an effective length of around 180 km and an effective width of around 90 km (**Fig. 2**).

3. Methodology

If we know the parameters that characterize a system and its initial (and boundary) conditions, then we can predict the behavior of the system at any instant of time. This type of problem, to predict future behavior, is called the

Table 2. Hypocentral parameters from NEIC.

Parameter	Value
Date	Aug. 15, 2007
GMT time	23:40:57
Latitude	-13.39°
Longitude	-76.60°
Depth	39 km
Magnitude	M_w8.0

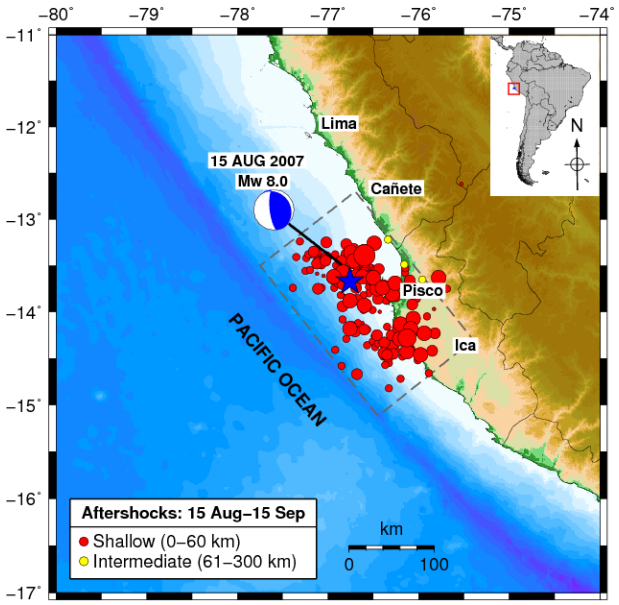

Fig. 2. Aftershocks of the earthquake. The rupture geometry is observed. Data is taken from USGS-NEIC.

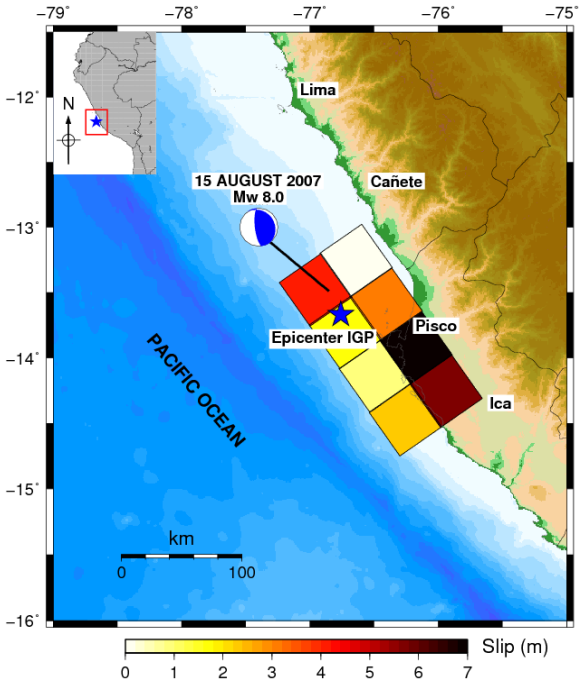

Fig. 3. Slip distribution of unitary seismic sources.

Table 3. Global CMT focal mechanism parameters.

Focal mechanism	Angle
Strike angle	325°
Dip angle	18°
Rake angle	63°

"direct problem." The "inverse problem" is to use the results of certain observations to infer the values of the parameters characterizing the system [12]. In this research, the tidal gauge records of tsunami will be used to infer the seismic source parameters and slip distribution.

The process will be considered as a "Linear and Time-Invariant System," which has two important properties: a) linearity, which allows using the superposition principle for Green's functions and for unitary deformations and b) invariance in time, that allows a shift in the time of the observed signals and their corresponding Green functions, synchronizing signals observed so that the tsunami arrival time corresponds to 20th minute, only for calculation purposes. This last point makes possible the use of tidal stations regardless of their distance from the epicenter. The solution of the inverse problem is not unique, but the set of values that provide the best correlation between observed and simulated data is chosen.

3.1. Source Parameters

To estimate the slip distribution, the inversion method for 10 tsunami waveform of good quality was used [13]. The rupture geometry was divided into 8 sub-sources (fragments) of identical dimensions: of length $L = 45$ km and of width $W = 45$ km, located at a depth H_j with respect to the upper side (in the vertical coordinate) of each sub-source (**Fig. 3**).

$$H_j = h + \frac{W}{2}\sin\delta \times [1 - \mathrm{mod}\,(j,2)], \quad j = 1,\ldots,8 \qquad (1)$$

$$h = h_e - [(x_e - x_0)\cos\theta - (y_e - y_0)\sin\theta]\tan\delta \qquad (2)$$

Where h is the depth of the upper side of the rupture area, x_0 and y_0 are the coordinates of the lower left corner, j represents the position of the j^{th} sub-source, δ is the dip angle, $\mathrm{mod}(j,2)$ represents the module or rest of j with respect to 2, (x_e, y_e, h_e) are the coordinates of the hypocenter and θ is the azimuthal angle. It should be noted that H_j is not the focal depth, but is related by Eq. (2).

The coseismic deformation is calculated for each sub-source with a unitary slip using Okada (1985) [14] formulation and focal mechanism data. The parameters of the focal mechanism are taken from Global CMT [15] and are equal for each sub-source (**Table 3**).

3.2. Green Functions Calculation

From the physical point of view, a Green's function represents the response of the system (simulated signal in the

Table 4. Slip distribution for each of the 8 sub-sources. The coordinates correspond to the lower left corner and the depth corresponds to the upper side (on the vertical axis) of the respective source.

N	Lat (°)	Lon (°)	H_j (km)	Slip(m)
1	-14.750	-76.300	14.00	2.3
2	-14.533	-75.983	27.91	5.7
3	-14.417	-76.533	14.00	0.8
4	-14.200	-76.217	27.91	7.0
5	-14.083	-76.767	14.00	1.7
6	-13.867	-76.450	27.91	3.1
7	-13.758	-77.000	14.00	4.1
8	-13.533	-76.683	27.91	0.1

i^{th} station) when the system is disturbed by a unit impulse (deformation due to a unitary slip in the j^{th} sub-source). Using this deformation field as initial condition, the waveforms (or Green functions) are calculated at each station simulating the propagation of tsunami waves by a finite difference method for each of the sub-sources, using an actual bathymetry. The tsunami waveforms observed are expressed as a linear combination of the tsunami waveforms calculated, in tensor notation:

$$G_{ij}(t) * m_j = d_i(t) \quad \ldots\ldots\ldots\ldots \quad (3)$$

where: $G_{ij}(t)$ is the Green function in the i^{th} station generated by the j^{th} sub-source, m_j is the value of slip at the j^{th} sub-source, $d_i(t)$ is the observed signal at the i^{th} station.

The linear tsunami propagation model TUNAMI in spherical coordinates was used [16], with a single rectangular grid to obtain the Green's functions corresponding to the tidal stations of Chile and the DART buoy.

3.3. Inversion

The inversion technique is performed by the method of non-negative least squares [17]. This method compares the simulated signals with the observed signals and minimizes the squared residual:

$$\left| G_{ij} m_j - d_i \right|^2 \to 0 \quad \ldots\ldots\ldots\ldots \quad (4)$$

with the condition: $m_j > 0$. We must take only the part of the signal corresponding to the first period of the wave to avoid contamination problems such as signal reflection effects and local resonance due to bathymetry and morphology of the coast around each station. In this case, it was taken the time window from the 20^{th} minute to 60^{th} minute, for purposes of calculating the inversion.

This algorithm guarantees that all values of slip are positive, as a necessary condition from the physical point of view. However, mathematically this model is not the most optimal result with respect to the method of simple least squares. The results of the inversion process are shown in **Table 4**.

4. Results

4.1. Deformation Field

From the slip distribution (**Table 4**), the total deformation field is obtained as a linear combination of unitary deformations, which will be used as initial condition for tsunami propagation. The maximum slip located at the southern part of the rupture geometry in the sub-source No.04 is 7.0 m. This maximum slip explains the fact that the Lagunillas bay area is the one that suffered the greatest impact due to inundation because it lies within the sub-source 04. Additionally, according to geodetic data taken by the Geophysical Institute of Peru after the earthquake, a geodetic point in Punta Paracas moved up 0.50 m and 1.60 m to the west [18]. The maximum value of the vertical component of the initial coseismic deformation is 1.53 m, located SW from Paracas, on the sea.

Table 5 shows the vertical deformation in some locations near the seismic source. For example, the cities of Cañete, Chincha and Tambo de Mora have suffered subsidence or downfall. Unfortunately, we don't have GPS measurements in these locations.

After the analysis of the position of the epicenter and the geometry of the rupture area, we can infer that the rupture process propagated in one way: from the epicenter (in the northern region of the geometry of rupture) to the south where there was the greatest deformation (**Fig. 4**). This is consistent with the results obtained by other methods such as teleseismic inversion [19] and teleseismic-geodetic inversion [20].

4.2. Scalar "Tsunami" Moment

Taking the slip distribution and dimensions of each sub-source, it can be calculated the scalar seismic moment, defined as:

$$M_0 = \mu L W D \quad \ldots\ldots\ldots\ldots \quad (5)$$

where: M_0 = seismic moment (Nm), $\mu = 4.0 \times 10^{10}$ N/m^2 average rigidity of elastic medium, $L = 180$ km total length of the source, $W = 90$ km total width of the source, $D = 3.07$ m, slip average. The scalar seismic moment is $M_0 = 1.99 \times 10^{21}$ Nm, according to the relation:

$$M_w = \frac{2}{3} \log(M_0) - 6.07 \quad \ldots\ldots\ldots\ldots \quad (6)$$

A moment magnitude scale of M_w8.1 is obtained. This means that from the tsunami waveforms recordings yields a similar magnitude M_w that with the seismic records.

4.3. Tsunami Waveforms from Seismic Source Inversion

Figure 5 shows the results of the inversion by comparing simulated and observed waveforms. Note that for purposes of calculating the inversion, all signals are displaced in time with respect to time of arrival at the respective station, so that all arrival times are synchronized on 20^{th} minute. We noticed that observed and simulated waves

Table 5. Vertical deformation Uz in some locations near the seismic source: uplift (+) or subsidence (−). We don't have geodetic observations for these locations, except for Punta Paracas (+50 cm).

Location	Lat (°)	Lon (°)	U_z (cm)
Cañete	-13.0777	-76.3874	-04.3
Chincha	-13.4048	-76.1270	-22.1
Tambo de Mora	-13.4604	-76.1768	-14.8
Pisco	-13.7099	-76.2031	38.9
Paracas	-13.8353	-76.2546	105.3
Independencia	-14.2791	-76.1982	111.8

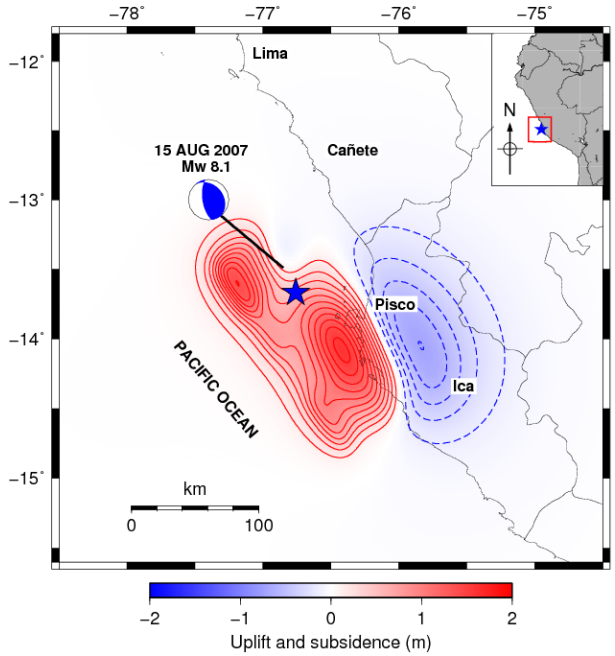

Fig. 4. Vertical component of the initial coseismic deformation.

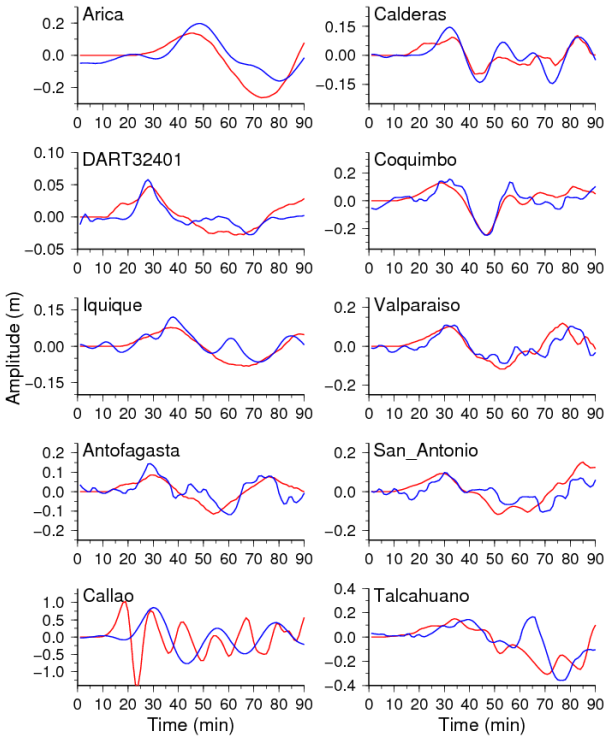

Fig. 5. Comparison of tide gauge records. In blue: observed signals, in red: simulated signals. Height (m) vs. Time (min). The time is synchronized for all records with respect to arrival time on 20th minute.

Table 6. Correlation coefficient between observed and simulated signals.

N	Station	Correlation
1	Arica	0.82
2	DART 32401	0.79
3	Iquique	0.78
4	Antofagasta	0.70
5	Callao	0.01
6	Calderas	0.82
7	Coquimbo	0.85
8	Valparaíso	0.80
9	San Antonio	0.70
10	Talcahuano	0.56

are well correlated (as shown in **Table 6**). **Table 6** shows the correlation coefficients between the observed signals and the simulated signals for each station. The stations of Coquimbo, Arica and Calderas have the best correlation. These correlations would improve if DART buoys (located at deep sea) were included in the inversion process, because there not would be problems of reflection and coastal resonance. However, the lack of coverage of these buoys in the western South Pacific and the large epicentral distance from the rest of these buoys would cause computing problems when working on far field simulation. For example, the dispersion effects are appreciable for far field simulation and this is a non linear problem. We have bypassed stations of Marcona and Juan Fernandez because they have a low correlation between simulated and observed signals.

4.4. Kinematic Effect of Seismic Source

The kinematic effects of the seismic source are appreciable if the rupture process is very slow ($v_r < 1.5$ km/s) and if the effective length of rupture is high, as the case of the Sumatra tsunami of 2004 that had a unidirectional rupture mode from south to north, with an effective rupture length of $L_{ef} \approx 1000$ km [21].

In the case of Pisco 2007 tsunami, the rupture process lasted a time τ around 2 minutes [5], so we can estimate the average rupture velocity from:

$$v_r = \frac{L_{ef}}{\tau} \quad . \quad . \quad . \quad . \quad . \quad . \quad . \quad . \quad . \quad . \quad . \quad . \quad . \quad . \quad (7)$$

As the rupture process mode is unidirectional from north to south: $L_{ef} = L$, then $L_{ef} \approx 180$ km, therefore: $v_r \approx 1.5$ km/s. However, Sladen et al. (2010) [20] argues that the Pisco event should not be considered a "tsunami

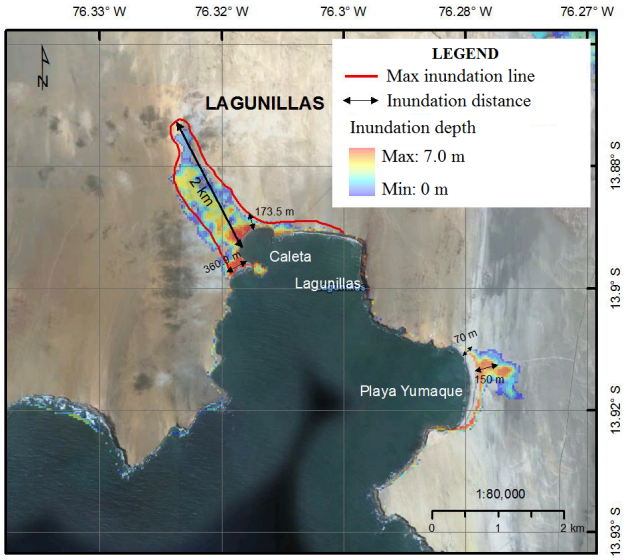

Fig. 6. Tsunami inundation map for Lagunillas and Yumaque (southern part of Paracas). In red: maximum inundation line from DHN tsunami survey [2].

Table 7. Maximum horizontal inundation obtained from numerical simulation compared with field survey observations from DHN [22].

Lat (°)	Lon (°)	Observed distance (m)	Simulated distance (m)	Error (%)
-13,4611	-76,1861	171	173	1.2
-13,4691	-76,1902	103	101	1.6
-13,6975	-76,2203	759	758	0.1
-13,7100	-76,2183	317	318	2.6
-13,7177	-76,2222	309	310	1.6
-13,7272	-76,2230	120	126	5.3
-13,7361	-76,2258	156	150	3.8
-13,7452	-76,2283	141	140	0.7
-13,8325	-76,2486	90.4	96	6.2
-13,8455	-76,5330	191	218	14.0
-13,8927	-76,3138	2000	1963	1.8
-13,8858	-76,3227	360	375	3.32
-13,8919	-76,3119	174	150	13.5
-13,9080	-76,2843	70	60	14.3

earthquake" despite the apparent slow rate of rupture, in this case should be interpreted that the earthquake consists of 2 sub-events, each one with a conventional speed (2 to 4 km/s), separated by a time of 60 seconds.

The rupture velocity is a parameter used to take into account the kinematic effect of the seismic source, so in this case, we will not take into account this effect, otherwise, we would simulate the seabed deformation sequentially and this would affect the propagation and inundation process.

4.5. Tsunami Propagation and Inundation

To simulate the propagation process of the tsunami, TUNAMI model was used. This model integrates the equations of linear shallow water theory by central finite difference numerical scheme.

With the seismic source obtained, the simulation was performed again for the nonlinear model, after performing the inversion, to verify that simulated signals obtained with the inversion process is correlated with the observed signals.

With respect to the directivity of the tsunami waves: the most of the energy is directed to the west, towards New Zealand and Australia. This directivity is determined by the perpendicular direction to the length of the fault plane and the bathymetry of the Pacific Ocean.

The most remarkable horizontal inundation took place in Lagunillas and was around 2 km (**Fig. 6**). The inundation distances (black arrows in **Fig. 6**) belong to the field survey observations of DHN [22]. According to the report of the DHN, the people mentioned that the first wave would have arrived 15 to 20 min after the earthquake, the second wave (which arrived after 10 to 15 min) was the highest and destructive. People report that the first wave came up to his knees when they were inside their homes and the second wave covered the roof of the houses. In this area three adults died. For Yumaque beach, the maximum run-up was reported by Woodman (2007) [23] and was around 10 m above the highest tide of the day; while the maximum inundation distance was around 150 m.

The maximum inundation distances and run-up can be used for validation of the seismic source model. If the difference between the observed and modeled results is too large, then either the model or the input data (in most cases) should be improved. This could include obtaining a better resolution bathymetric and topographic data and a better model of the seismic source. The requirements to reduce errors between observed and simulated parameters vary from one model to another.

Table 7 shows the comparison of the simulation results versus field survey observations from DHN. For example, in the case of Lagunillas, the maximum inundation observed was 2000 m (according to DHN) and the simulated distance was 1963 m with an error of 1.8%. This is a very good correlation and shows that the seismic source model works very well.

5. Conclusions

The solution of the inverse problem is not unique, but we used slip values that provide the best correlation between observed and simulated tsunami waveforms.

The maximum amplitude of the initial coseismic deformation model is 1.53 m. The maximum slip is 7.0 m and it is located in the southern part of the rupture area, specifically, south of the Paracas Peninsula. This fact and the horizontal slope topography in Caleta Lagunillas explain the great horizontal inundation of around 2 km.

The results of the deformation field show that the cities of Cañete, Chincha and Tambo de Mora have suffered subsidence or downfall, while the cities of Pisco and Para-

cas have suffered uplift.

It is important to have good azimuthal distribution of tide gauge stations around the seismic source geometry. Furthermore, the result will depend on the quality of the tide gauge data and quality of the local bathymetry around each station.

The rupture process, whose beginning was at the epicenter, presented a unidirectional directivity along the azimuth from north-west to south-east. There are two principal asperities, the greater one is concentrated on southern of the Paracas Peninsula. This is in agreement with the teleseismic body waveform inversion.

The scalar seismic moment calculated is $M_0 = 1.99 \times 10^{21}$ Nm and the magnitude of the earthquake inferred from tide gauge records is M_w8.1. Same as the magnitude obtained from teleseismic waveform inversion.

One way to verify the seismic source model proposed is by comparing the observed and simulated tsunami waveform. The tidal stations in Coquimbo, Arica, Calderas and Valparaiso have the highest correlation values, while Callao, Marcona, Juan Fernandez and Talcahuano have a low correlation value.

The proposed model is not good in the near field region because the correlation values are low in Callao and Marcona. So, additional studies are required to improve the seismic source model and bathymetry data for tsunami inversion in near-field region.

The most remarkable horizontal inundation took place in Lagunillas and was around 2 km. Comparing with the field survey observation, there is an error of 1.8%, so, the seismic source model works very well.

Acknowledgements

The authors acknowledge support from: the project of Science and Technology Research Partnership for Sustainable Development supported by JST-JICA, the Dirección de Hidrografía y Navegación of the Peruvian Navy and the Universidad Nacional Mayor de San Marcos – FENLAB.

References:

[1] C. Jiménez, N. Moggiano, and M. Saavedra, "Fuente sísmica del terremoto de Pisco 2007 a partir de inversión de registros mareográficos," Revista de Investigación de Física UNMSM, Vol.15, No.2, 2012.
[2] N. Moggiano, "Modelado Numérico del Maremoto de Pisco 2007," Tesis de Licenciatura, Universidad Nacional Mayor de San Marcos, Peru, 2013.
[3] E. Norabuena, T. Dixon, S. Stein, and C. Harrison, "Deceleration and Nazca-Pacific plate motions," Geophysical Research Letters, Vol.26, pp. 3405-3408, 1999.
[4] E. Silgado, "Historia de los Sismos más notables ocurridos en el Perú (1513-1974)," Boletín No.3. 1978. Instituto de Geología y Minería. Lima, Perú.
[5] H. Tavera and I. Bernal, "The Pisco (Perú) Earthquake of 15 August 2007," Seismological Research Letters. Vol.79, No.4, pp. 510-515, 2008.
[6] IOC (International Oceanographic Center). Sea Level Station Monitoring Facility. Web: http://www.ioc-sealevelmonitoring.org/ [accessed Dec. 2012]
[7] NOAA, National Data Buoy Center. Web: http://www.ndbc.noaa.gov/dart.shtml [accessed Dec. 2012]
[8] C. Jiménez, "Procesamiento digital de señales sísmicas con Matlab," Revista de Investigación de Física, UNMSM, Vol.10, No.2, pp. 23-28, 2007.
[9] A. Rabinovich, R. Thomson, and F. Stephenson, "The Sumatra Tsunami of 26 December 2004 as observed in the North Pacific and North Atlantic oceans," Surv Geophys, Vol.27, pp. 647-677, 2006.
[10] GEBCO, General Bathymetric Chart of the Oceans. Web: http://www.gebco.net/ [accessed Dec. 2012]
[11] USGS, Nacional Earthquake Information Center. http://neic.usgs.gov [accessed Jan. 2013]
[12] A. Tarantola, "Inverse problem theory and methods for model parameter estimation," Ed. Society for Industrial and Applied Mathematics. Philadelfia, 2002.
[13] K. Satake and H. Kanamori, "Use of tsunami waveform for earthquake source study," Natural Hazards Vol.4, pp. 193-208. 1991.
[14] Y. Okada, "Surface deformation due to shear and tensile faults in a half space," Bulletin of Seismological Society of America, Vol.75, No.4, pp. 1135-1154, 1985.
[15] G. Ekström and M. Nettles, "Global Centroid Moment Tensor Project," Columbia University. Web page: http://www.globalcmt.org/ [accessed Jan. 2013].
[16] F. Imamura, "Review of Tsunami Simulation with a Finite Difference Method. Long Waves Runup Models," World Scientific Publishing Co. Pte. Ltd. Singapore, 1996.
[17] C. Lawson and R. Hanson, "Solving Least Squares Problems," Prentice–Hall, 1974.
[18] L. Ocola, Aspectos físicos del maremoto de Pisco del 15 de agosto de 2007 y las inundaciones máximas. Vol.: El terremoto de Pisco del 15 de agosto de 2007 (M_w7.9). Instituto Geofísico del Perú.
[19] C. Ji and Y. Zeng, http://earthquake.usgs.gov/earthquakes/ eqinthenews/2007/us2007gbcv/finite_fault.php [accessed Dec. 2012]
[20] A. Sladen, H. Tavera, M. Simons, J. Avouac, A. Konca, H. Perfettini, L. Audin, E. Fielding, F. Ortega, and R. Cavagnoud, "Source model of the 2007 M_w8.0 Pisco, Peru earthquake: Implications for seismogenic behavior of subduction megathrusts," Journal of Geophysical Research, Vol.115, B02405, 2010.
[21] A. Suppasri, F. Imamura, and S. Koshimura, "Effects of the rupture velocity of fault motion," Coastal Engineering Journal, Vol.52, No.2, pp. 107-132, 2010.
[22] DHN. Informe Post Tsunami Pisco 2007. Dirección de Hidrografía y Navegación, Marina de Guerra del Perú (2007). https://www.dhn.mil.pe/docs/tsunami/Informe_Post_Tsunami_Pisco%202007.pdf [accessed Jan. 2013]
[23] R. Woodman, "Observaciones del tsunami asociado con el Terremoto de Pisco del 15 de Agosto 2007, en El terremoto de Pisco (Peru) del 15 de Agosto de 2007," Instituto Geofísico del Perú, pp. 351–362.

Name:
Cesar Jimenez Tintaya

Affiliation:
Fenlab, Universidad Nacional Mayor de San Marcos (UNMSM)
Dirección de Hidrografía y Naveagacíon (DHN)

Address:
Av. Venezuela s/n, Lima, Perú
Calle Roca 116, Chucuito-Callao, Perú

Brief Career:

2000-2007 Assistant Research, Instituto Geofisico del Perú IGP
2008-2014 Research Scientist, Dirección de Hidrografía y Naveagacíon
2009-2014 Assistant Professor, UNMSM, Perú
2014- Master in Geophysics, UNMSM, Perú

Selected Publications:

• M. Ioualalen, H. Perfettini, S. Yauri, C. Jimenez and H. Tavera, "Tsunami Modeling to Validate Slip Models of the 2007 M_w8.0 Pisco Earthquake, Central Peru," Pure and Applied Geophysics. 2012.
• E. Mas, S. Koshimura, A. Suppasri, M. Matsuoka, M. Matsuyama, T. Yoshii, C. Jimenez, et al. (2012). "Developing Tsunami fragility curves using remote sensing and survey data of the 2010 Chilean Tsunami in Dichato," Natural Hazards and Earth System Science, 12, 2689-2697. doi:10.5194/nhess-12-2689-2012.
• T. Yoshii, M. Imamura, M. Matsuyama, S. Koshimura, M. Matsuoka, E. Mas and C. Jimenez. "Salinity in Soils and Tsunami Deposits in Areas Affected by the 2010 Chile and 2011 Japan Tsunamis," Pure and Applied Geophysics, 2012.

Academic Societies & Scientific Organizations:

• Peruvian Society of Physics (SOPERFI)